End-Terminated Poly(urethane−urea) Hybrid Approach toward Nanoporous/Microfilament Morphology

Rashmi Edachery Veetil, Bhuvaneswari Soundiraraju, Dona Mathew, and Santhosh Kumar Kalamblayil Sankaranarayanan*

Cite This: ACS Omega 2022, 7, 6280−6291

Read Online

ACCESS | Metrics & More | Article Recommendations | Supporting Information

ABSTRACT: In the present work, the effect of heteroatomic hydrogen bonding on the properties of −OH/−NH-terminated soft-segment-free polymers, viz, polyurethane (P-UT), polyurea (P-UR), and their hybrid (P-UT−UR), is explored. P-UT was synthesized from phloroglucinol and P-UR was synthesized from 1,3,5-triazine-2,4,6-triamine by employing hexamethylene diisocyanate as a counterpart. P-UT exhibited a spherulitic structure with varying sizes, whereas P-UR displayed a fibrillar structure characteristic as that of crystalline hard segments. The P-UT−UR hybrid exhibited a fine nanospherulitic structure with a high order of interconnectivity. Negative surface skewness values of −0.47 and −0.18 were measured (by AFM) for P-UT and P-UT−UR, respectively, which revealed that the surface is not smooth and is covered with features. Due to the increased H-bonding (−N−H···O−H) in P-UT−UR, its transparency decreased. A block copolymer hybrid of urethane−urea was synthesized, which preferred homoatomic H-bonding, whereas random urethane/urea bridges favored hetreoheteroatom H-bonding. A pentafluorophenyl end-functional hybrid (PFI−P-UT−UR) was synthesized, which displayed filaments of ∼2−3 μm length in contrast to the interconnected nanospherulitic structure observed for P-UT−UR. The self-aggregation and end folding led to the formation of a filament structure. By altering the chemical structure slightly, nano-ordered polyurethanes or their hybrids can be achieved.
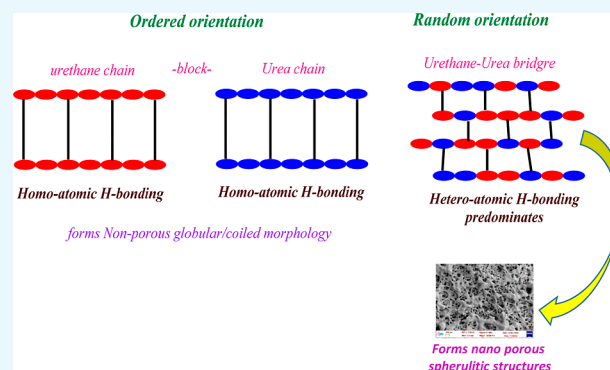
1. INTRODUCTION

Polyurethanes (P-UTs) and polyureas (P-Us) are multipurpose materials. They find wide applications in diverse fields such as textile fibers, biomaterials, membranes, coatings, and adhesives.[1−3] They generally comprise a relatively flexible component (soft segment) and a relatively polar/stiff component (hard segment). The hard−soft segment arrangement is the prime impetus for the peculiar morphology of P-UTs.[4,5] The thermodynamic incompatibility between segments offers microphase separation.[6,7] However, P-UTs derived without using a soft segment have seldom been investigated (soft-segment-free P-UTs).[8−13] The morphology changes in these polymers do not depend much on the hard−soft segment topology concept (seen in conventional P-UTs) but on other factors. Secondary forces such as hydrogen bonding play a key role in dictating the microstructure of macromolecules. H-bonding between polymer chains leads to microphase separation, which in turn changes the morphology of polymers.[14−16] The soft-segment-free P-UTs attract great interest as they enable easy manipulation of morphology and a more in-depth understanding of the supplementary role played by secondary forces in P-UTs.

Goddard et al. synthesized P-UTs with hard segments that had pendant trialkylammonium groups quaternized with alkyl halides. The P-UT cationomers thus formed showed better microphase separation and superior mechanical properties than their nonionic precursors due to strong interurethane hydrogen bonding between the carbonyl and the urethane −N−H groups in the cationomer.[17] In one of the studies, it was found that the hydrogen bonding between two urethane moieties (or two urea moieties) improves the microphase separation.[18] Heteroatomic H-bonding between electronegative atoms such as nitrogen or oxygen and hydroxyl groups displays enhanced properties than those exhibited between hydroxyl groups. This is achieved by the addition of heteroatomic molecules equipped with additional hydrogen-acceptor moieties.[19,20] The increased strength of heteroatomic hydrogen bonding when compared to homoatomic hydrogen bonding is

associated with the increased delocalization energy of lone pairs of heteroatoms. It is known that larger delocalization energies correspond to stronger H-bonds.[21] Formation of these kinds of multiple hydrogen bonds not only increases the strength of the interaction but also affords unique hydrogen-bonded architectures. The thermal and physical properties of epoxy resin were enhanced by embedding a heteroatom containing a hydrogen acceptor, to induce multiple hydrogen bonding.[22,23] In the work of Zhu et al., hydrogen bonding was utilized to improve the miscibility between unsaturated polyester and epoxy networks by inserting bisphenol A, which contains strong electronegative atoms and therefore forms strong heteroatomic H-bonds. The same functional group can form multiple hydrogen bonds depending on the donor/acceptor molecule employed and also on the multiple sites capable of engaging these intermolecular interactions.[24]

During the studies of hydrogen bonding in thiophenols, David and Hallam found the presence of stronger hydrogen bonding in S−H···O and S−H···N and least hydrogen bonding in S−H···S, using FTIR spectroscopy.[25] In another report, it was found using STO-3G ab initio studies that C═O···H−N has a stronger relative stability (9.4 kcal/mol), followed by amide−H_2O (7.4 kcal/mol), and least stability for H_2O−H_2O (6.5 kcal/mol).[26]

Heteroatomic H-bonding also leads to polymer chain self-assembly and influences the solid-state morphology of a polymer material. These strong supramolecular interactions can modify the thin film morphology too. In the work of Ocheje et al., the solid-state morphology of conjugated polymers (based on diketopyrrolopyrrole) was modulated by incorporating amide-containing alkyl side chains. The intermolecular hydrogen bonds formed between adjacent amide moieties directly affected the lamellar packing of the polymer and aggregation, without affecting the π-conjugation. It is reported that the change in the pore size and shape occurs due to the presence of heteroatomic H-bonding.[27] The presence of heteroatomic H-bonding increases the pore size and decreases the number of pores due to their strong interaction. Transformation of nanofibers to nanospheres was achieved via heteroatomic H-bonds.[23] Because supramolecular interactions can be formed and broken reversibly under a variety of external conditions, supramolecular copolymer thin films with a cylindrical morphology can potentially give rise to nanoporous membranes featuring recognition sites arrayed within the nanopores.

End-group functionalization of polymers would facilitate a wide range of applications by permitting the way for block copolymers, attachment of specific active groups, access of building blocks for supramolecular self-assembly units, and so on.[28] P-UTs can be synthesized as end-functionalized macromolecules, and later the chain ends can be terminated with appropriate molecules to result in end-terminated P-UT. These materials having different terminal structures will have different morphologies and properties. In end-terminated P-UTs, polymer chain ends will have more degrees of freedom and can undergo surface modification through the formation of the molecular overlayers produced by chain folding and alignment/packing of adjacent chains.[22,29] Terminal −OH groups were found to associate in dynamic aggregates of various sizes. To cite some examples of end-terminated polymers, pentafluorobenzene (PFB) end-capped poly(3-octyl) thiophene exhibited excellent solubility in a range of polar solvents, bearing rapid "click"-type nucleophilic aromatic substitutions

at ambient temperature.[30] End-group-functionalized polymer brushes were synthesized with bromide-terminated poly-[oligo−(ethylene glycol)methyl ether methacrylate], which under mild conditions were used for the transformation of the polymer end-groups into cyclopentadiene having excellent antifouling properties.[31] A P-UT-based prepolymer which was further end-capped with strong hydrogen bonding ureidopyrimidinone, pyrimidinedione, and ethanol groups led to an increase in mechanical properties. The quadruple hydrogen bonding was found to be capable of increasing the mechanical properties and also the toughness.[32]

In this work, end-functional P-UT, poly(urea) [P-UR], and the poly(urethane−urea) [P-UT−UR] hybrid are synthesized and their H-bonding orientations are studied. The effects of solvents on the morphology of polymers is investigated. End-terminated polymers are synthesized and their morphological differences are recorded using field emission-scanning electron microscopy (FESEM) and atomic force microscopy (AFM). The surface aggregation behavior of end-functional and end-terminated polymers is tracked by contact angle (CA) measurements. Block polymers (urethane-*block*-urea) are synthesized to observe the surface morphology change vis-à-vis the random (urethane-*ran*-urea) macromolecule.

2. RESULTS AND DISCUSSION

2.1. Synthesis and Characterization of P-UT, P-UR, and P-UT−UR Polymers.
Initially, −OH functional P-UT, −NH_2 functional P-UR, and −OH/−NH_2 functional P-UT−UR were synthesized, and final polymers were obtained by precipitation/drying. On comparing the FTIR spectra (Figure 1) of P-UT, P-UR, and P-UT−UR, the stretching frequency in
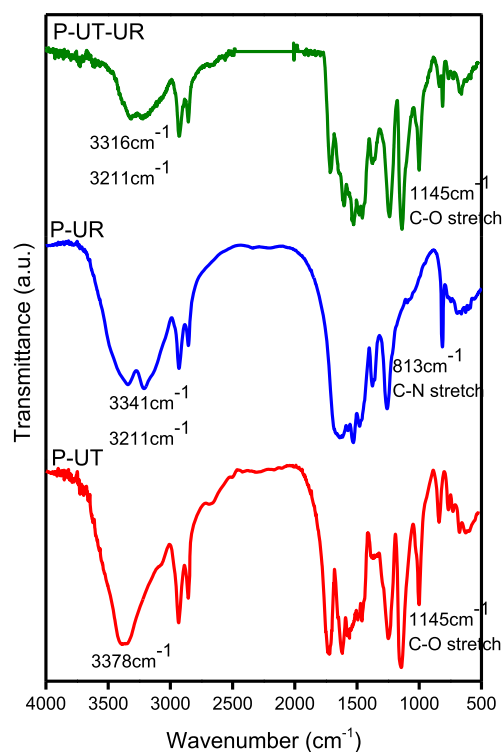
Figure 1. FTIR spectra of P-UT, P-UR, and P-UT−UR indicate the splitting of peaks in P-UR and P-UT−UR in the region 3300−3500 cm^{-1}. A broad peak at 3378 cm^{-1} is attributed to hydrogen bonded −OH groups.
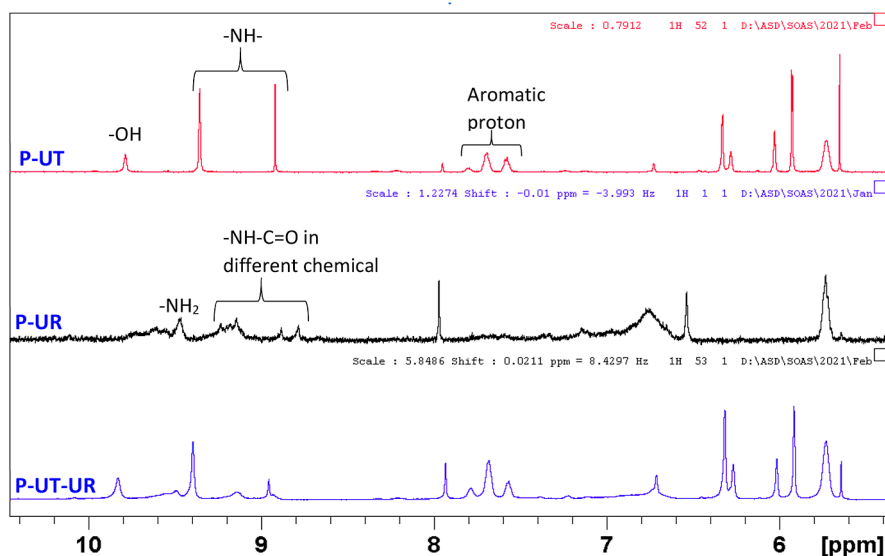
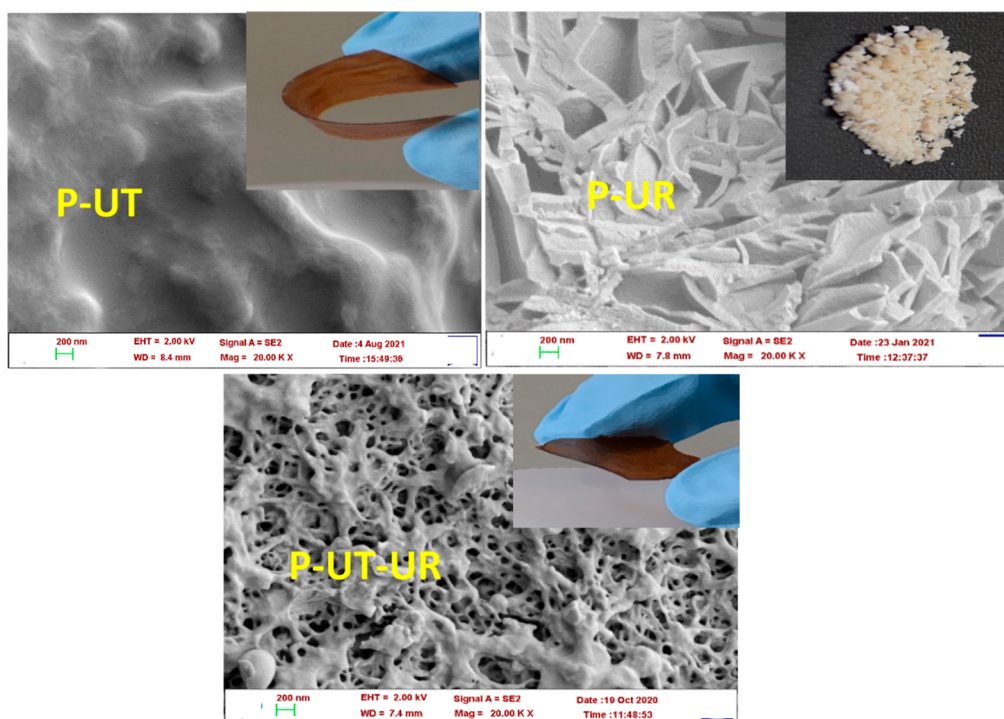**Figure 2.** Proton NMR spectra of P-UT, P-UR, and P-UT−UR.

Figure 3. FESEM images of P-UT, P-UR, and P-UT−UR. P-UT−UR features a fine porous web-like morphology.

the C═O and C−N region supports the formation of urethane and urea bridges, respectively, in the polymers. In P-UT, a broad single peak at 3378 cm^{-1} indicates the presence of hydrogen-bonded −OH groups. In P-UR, the peaks that appeared as a doublet (split) at 3341 and 3211 cm^{-1} indicate the presence of −NH and end-functional −NH$_2$ groups. In P-UT−UR, the broad multiple peaks observed at 3316 and 3211 cm^{-1} endorse the presence of both hydrogen-bonded −OH and −NH groups. The H-bond possibilities in P-UT, P-UR, and P-UT−UR are between −O−H···O−H−, −N−H···N−H−, and −N−H···O−H− respectively.

Formation of the products was further confirmed from the proton NMR spectra (Figure 2). From the NMR spectra, all the functional groups are recognized from their corresponding

peaks. The peak of the highly H-bonded end-located −OH group in P-UT is observed at δ = 9.8 and the peaks of H-bonded −NH are noted at δ = 9.4 and δ = 8.9, respectively. In P-UR, the peaks of the end-located −NH$_2$ groups are observed at δ = 9.5. Signals at δ = 9.2, 8.9, and 8.8 correspond to −NH−C═O in different chemical environments. The H-bonded protons are more deshielded due to a decrease in electron density over the proton. As P-UT−UR is a hybrid of P-UT and P-UR, all the signals are retained in the hybrid spectra vis-à-vis P-UT/P-UR alone. The shift in the values of −OH, −NH, −NH−COO indicates the presence of H-bonding. Non-hydrogen-bonded −OH (δ = 9.0) shifted to δ = 9.8 due to H-bonding. The same is the case for the NH$_2$ group (δ = 6 is shifted to δ = 9.5).
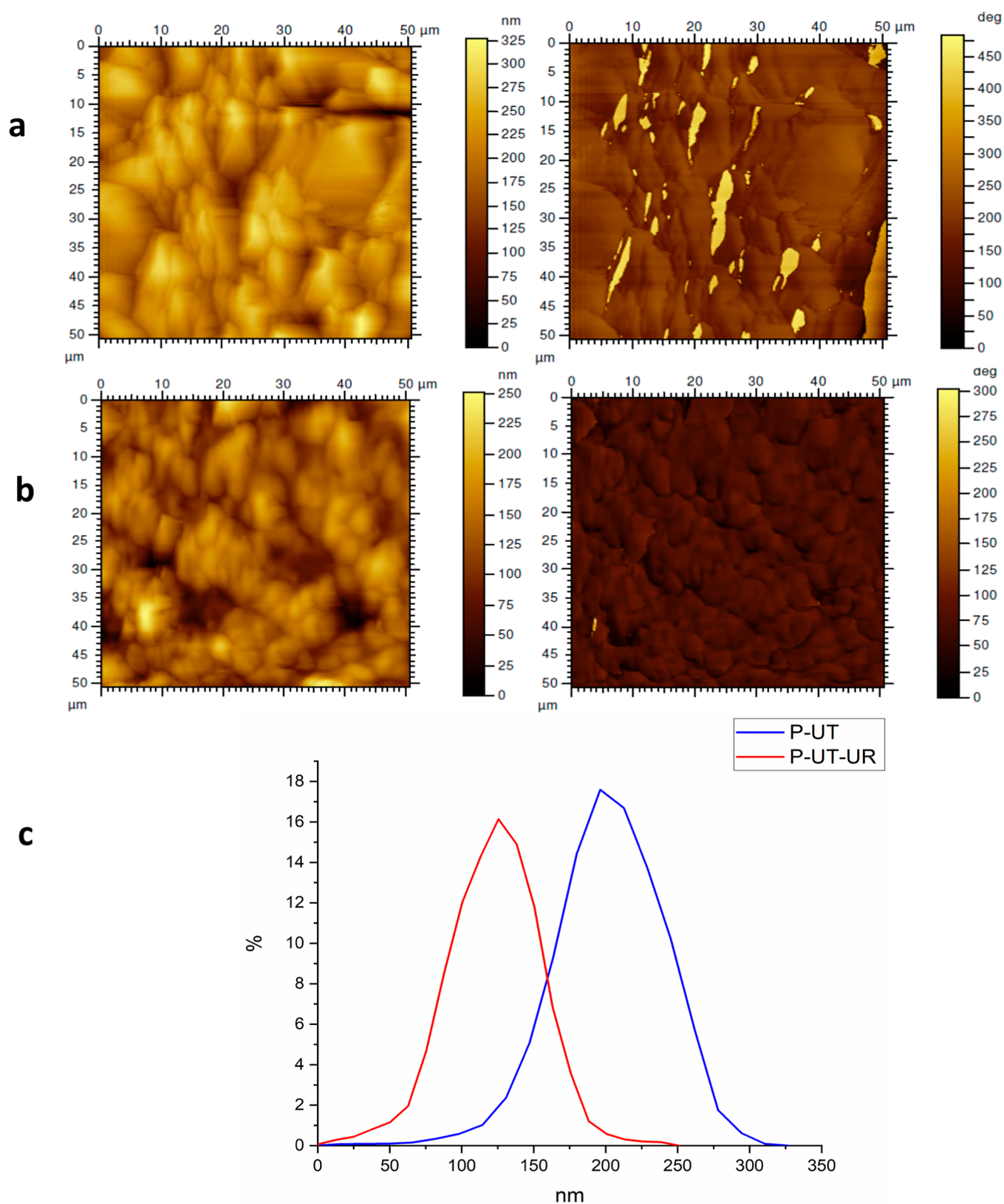
Figure 4. Topography and phase images of (a) P-UT and (b) P-UT−UR films obtained using AFM studies and (c) histogram profile showing the particle size distribution in polymers.

To see the changes in key thermophysical properties, glass transition temperature of polymers was determined by the differential scanning calorimetry (DSC) method (Figure S1a). The T_g values were found to be 90, 178, and 100 °C for P-UT, P-UR, and P-UT−UR, respectively. Also, the softening points of the polymers were 134, 171, and 145 °C for P-UT, P-UR, and P-UT−UR, respectively (softening point apparatus method, Figure S1b). The film-forming tendency of all the

polymers was examined physically. It is noted that P-UT is capable of forming transparent and reasonably good flexible films (solvent-borne and by heating/pressure at 150 °C). P-UR could not form a film by both preparation methods, and it merely remained as a powder. Meanwhile, hybrid P-UT−UR formed a brittle transparent film (by both preparation methods) (Figure 3 inset).

The FESEM images of the synthesized polymers (Figure 3), P-UT, P-UR, and P-UT−UR, revealed that morphologies of the polymers varied significantly with respect to the chemical structure and H-bonding. P-UT exhibited a spherulitic structure with varying sizes, whereas P-UR displayed a fibrillar structure characteristic of that of crystalline hard segments.[33] Interestingly, P-UT−UR exhibited a fine nanospherulitic structure with a high order of interconnectivity, which could possibly be attributed to the varying degrees of H-bonding in these polymers. To explore more about the morphology and phases of the polymers, AFM analysis was carried out in the contact mode and in the tapping mode. Figure 4a,b shows the topography and phase images of P-UT and P-UT−UR films, respectively. AFM analysis of P-UR could not be done due to the lack of the film formation tendency of the polymer. The observations from the topography images of P-UT and P-UT−UR were complementary to those of FESEM images with a spherulitic structure and an ordered interconnected nano-spherulitic structure. The phase images showed no evidence of the second phase, pointing to the existence of only a single phase corresponding to the hard segment. This infers that by changing the urethane and urea bridges in polymers (and hybridizing), polymer properties have significantly changed (vide infra).

From the topographic images, the surface roughness (S_a), roughness parameters (surface skewness and surface kurtosis), and particle size distributions were calculated. The surface roughness of P-UT was 29.7 nm, whereas that of the P-UT−UR film was 25.3 nm. Surface skewness (S_{sk}) is a measure of asymmetry of the profile about the mean plane and illustrates load carrying capacity, porosity, and characteristics of films. Negative S_{sk} values of −0.47 and −0.18 for P-UT and P-UT−UR revealed that the surface is not smooth and is covered with features. Surface kurtosis (S_{ku}) is a measure of the distribution of the features on the surface and is useful for evaluating randomness of surface heights. Surfaces with more random features possess a value of greater than 3.[34−36] S_{ku} of P-UT of 4.0 nm indicates that its surface is more random compared to that of P-UT−UR with a S_{ku} value of 3.6 nm, which also accounts for the higher S_a value noted for P-UT. The particle size distribution extracted from the topography image of P-UT is shown in the overlaid histogram profile (Figure 4c), which revealed that the particle sizes varied from ∼50 to 330 nm. The histogram profile of P-UT−UR pointed toward the existence of particles from ∼1 to 250 nm.

Subsequently, surface aggregation behaviors of polymers were explored. For this, interaction of polymers with water molecules with respect to time of contact was studied by static CA measurements (Figure 5a). Toward this, thin films (coating) of all the polymers were prepared by spray coating, and a water droplet of 5 μL volume was dropped over the polymer surface and CA was recorded for a duration of 300 s. In all cases, CA decreased with time. P-UT, P-UR, and P-UT−UR showed CA values of 113, 76, and 81° initially (0 s), which shifted to 109, 69, and 71°, respectively, after 300 s. This hydrophobic character of P-UT may be due to its highly

a)

b)
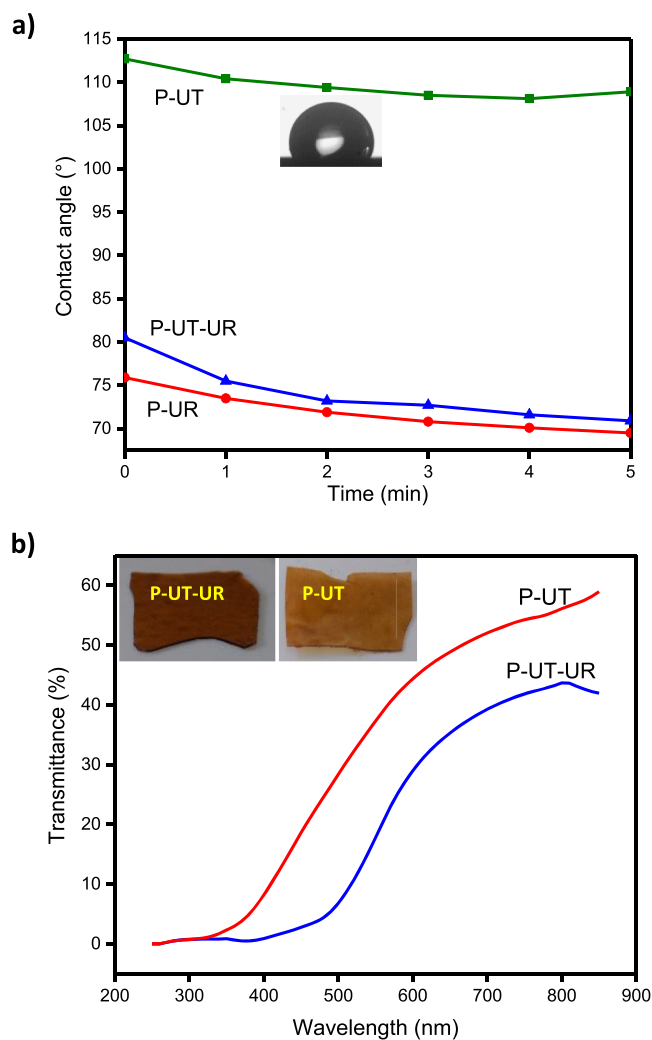
Figure 5. (a) CA of P-UT, P-UR, and P-UT−UR with respect to time of contact and (b) transparency of P-UT and P-UT−UR films.

compact structure, whereas decreased CA of P-UR and P-UT−UR may be due to more water-interacting groups such as NH−CO−NH− bonds. If H-bonding sites exist high in number, polymer chains will interact with water molecules (as it is a H-bonding molecule) instantaneously, which leads to a secondary surface orientation of the polymer chain. P-UT exhibited a drop in CA of 4°, P-UR exhibited a drop of 7°, whereas P-UT−UR recorded a dip of 10°. This indicates that P-UT−UR is more H-bonded compared to P-UT and P-UR. The reduction in CA is due to the surface orientation.[37] Another observation is P-UT is hydrophobic and the other P-UR and P-UT−UR are hydrophilic in character. Even after interaction with water, the polymers are retaining the hydrophobic/hydrophilic character (no shift from hydrophobic to hydrophilic is noted).

To see the impact of H-bonding, the UV−visible spectra of the P-UT and P (UT−UR) films (P-UR could not form a film) were recorded (Figure 5b). It is observed that both the P-UT and P (UT−UR) hybrids are able to absorb visible light. The maximum transparency of P-UT−UR (44%) is lower than that of P-UT (59%). This decrease in transparency of P-UT−UR is due to increased H-bonding (−N−H···O−H). If the structure has hydrogen bonding (more compact), light cannot be transmitted easily and will be trapped. Hence, transparency will
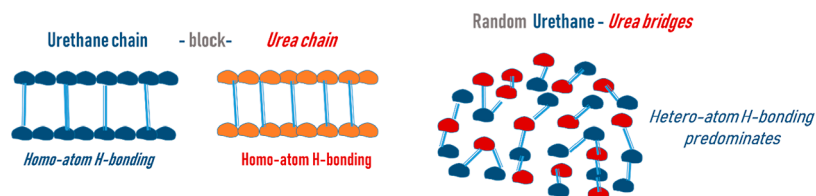
Figure 6. Schematic representation of hetero-/homoatomic H-bonding in BC-PUU and P-UT−UR hybrids.

be less. These studies clearly identified further the influence of H-bonding in these polymers.

It is interesting to see the reason for the formation of a nanoporous morphology in the P-UT−UR hybrid. The rationale can be the heteroatom hydrogen bonding. In the P-UT−UR hybrid, −NH−CO−NH (urea bridge) and −O-CO−NH− (urethane bridge) are present randomly as the reaction was carried out in one-shot. This random array of bridges may lead to a stabilized and more suitable orientation, resulting in a nanoporous morphology. The nanoporous nature can also be due to the bulkiness of groups, which pull apart the chains to provide porous nature.[19,38,39]

With a perception that the more ordered urethane and urea block will behave differently, their block copolymer was synthesized (two-step route). In this attempt, the block copolymer hybrid (BC-PUU hybrid) was synthesized by initially reacting hexamethylene diisocyanate with phloroglucinol for 3 h at 125 °C with continuous stirring under a N_2 atmosphere (P-UT chains are formed with −NCO end groups), followed by the addition of melamine solution to the reacting mixture to result polyurea block. After 2 h of reaction, the polymer was precipitated in ice cold water and dried under vacuum. On comparing the spectrum with that of P-UT−UR, the −OH peak shifted to a higher wavenumber (from 3316 to 3405 cm^{-1}) in the BC-PUU hybrid (Figure S2), which indicates the decrease in H-bonding of the −OH group. This result seems to be interesting as the blocks are formed (polyurethane block−poly urea block) in an ordered manner, the possibility of easy orientation and heteroatom H-bonding is restricted. This may be the rationale for reduction in H-bonding in the block hybrid. The FESEM image of the block-hybrid featured no special morphology (Figure S3). The alignment of polymer chains in BC-PUU is "regionally" ordered favoring homoatom H-bonding (Figure 6). They have more affinity for homoatomic H-bonding (−O−H···O−H or −N−H···N−H) due to the specific arrangement. The H-binding sites are randomly distributed in P-UT−UR such that they have more exposure to the strong heteroatomic H-bonding (−O−H···N−H). This piece of experiment clearly marks the efficacy of heteroatom H-bonding in polymers.

Solubility of all polymers was recorded by dissolving polymers in the DMF solvent. Intention of this study is to observe the difference in the solvent−polymer interactions. About 1.0 g of each polymer was attempted to dissolve in 3.0 mL of DMF at 125 °C (for 20 min). P-UT and P-UT−UR dissolved completely, whereas P-UR remained insoluble even for an extended time. The presence of free hydroxyl groups in P-UT and P-UT−UR may favor interaction with the polar DMF solvent resulting in dissolution. The more polar nature of the −OH group compared to that of −NH is the rationale here for difference in solubility. Extended H-bonding in P-UR may hinder the dissolution. To study the effect of solvents on the surface morphology via the hydrogen bonding difference, the polymers were interacted with selected solvents via immersion

(72 h). Most polar water (polarity index is 1.00) and least polar THF (polarity index 0.21) were employed for the study. Variation of the surface morphology was studied using FESEM imaging (Figure 7). We observed no morphology change or
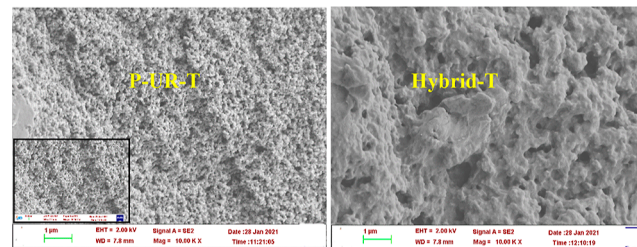
Figure 7. FESEM images of P-UR and P-UT−UR films in the THF solvent. Formation of voids due to the solvent−polymer interaction is observed.

unusual morphology for P-UT in any of the solvents. Meanwhile, P-UR (and hybrid) exhibited a porous morphology in THF. (However, polymers in water retained the fused globular structure.) Previous studies reported the formation of a porous morphology in the presence of solvents due to extensive H-bonding interactions. Also, with an increase in H-bonding capacity, the porosity of the polymer is also increased.[40−42] From the FTIR spectra of P-UT (Figure S4), P-UR (Figure S5), and P-UT−UR (Figure S6) in different solvents, it can be seen that no chemical reaction takes place in different solvents but physical interactions only take place.

The solubility parameter values of P-UTs are reported as δ_d = 18.1, δ_p = 9.3, and δ_h = 4.5.[43−45] By correlating the Hansen hydrogen bonding parameter (δ_h) of solvents (Figure S7) and P-UTs, it is found that δ_h values of THF and P-UTs are comparable and hence it can be viewed that highest H-bonding is possible in the THF−P-UT combination. Also, it supports the extensive morphology change and porosity in the THF solvent. The rationale for the porous morphology in P-UR-T may be the H-bonding interaction, followed by the fast evaporation of THF from the polymer in the drying process. The H-bonded THF residing in polymer chains will pull apart chains during the drying process. This H-bonded THF will escape on drying by leaving a porous morphology. Solvents exert a significant effect on the polymer morphology that the H-bonding between the solvent and polymer site can result in enhanced morphologies.[46−48] Several studies reported the formation of a porous morphology in the presence of solvents that can induce extensive H-bonding. With an increase in H-bonding capacity, porosity of polymers is increased.[49,50] There are studies that state the ability of proton-acceptor solvents such as THF to tune morphologies from long fibers to spherical aggregates. Wang et al. described the pathway-dependent self-assembly of peptide bola-amphiphiles in water with trace THF. The presence of trace THF (as a proton acceptor) changes the H-bonding network giving rise to tuned
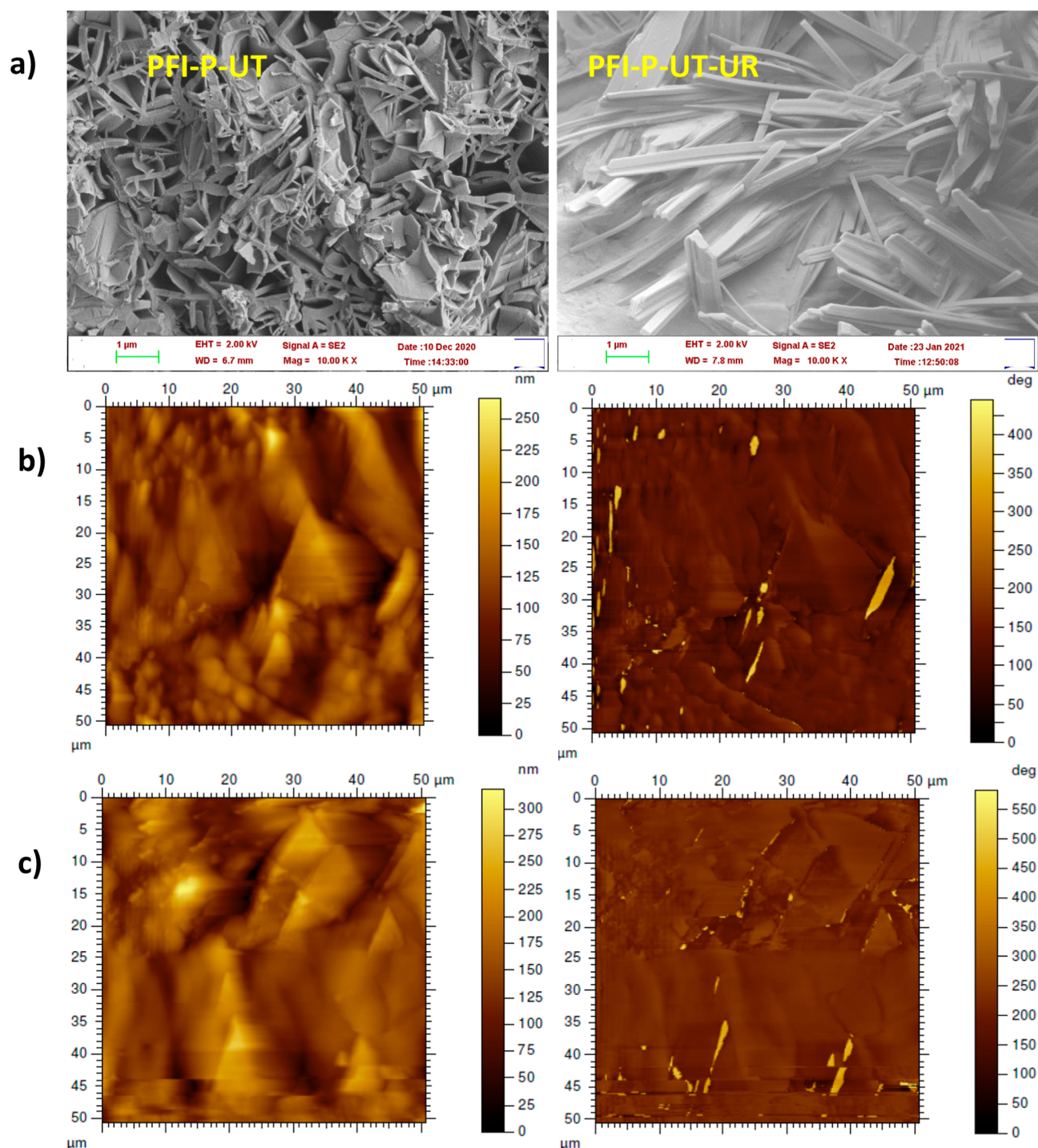
Figure 8. (a) FESEM images of PFI−P-UT and PFI−P-UT−UR and (b) topography and phase images of PFI−P-UT and (c) PFI−P-UT−UR from AFM.

morphologies from long fibers to spherical aggregates and resulted shifts in luminescence and hydrophobicity. When THF was replaced with ethanol, this property was lost.[51] P-UTs are highly capable of generating new chemical structures and supramolecular morphologies. The unique properties of P-UTs arise from the high degree of intermolecular hydrogen bonding.

2.2. Synthesis and Characterization of End-Terminated Polyurethane (PFI−P-UT) and Hybrid (PFI−P-UT−UR) Polymers. End-functional polymers can be end-terminated by the addition of reactive molecules and hence H-bonding in polymers can be altered. These subtle changes can have a massive impact on polymer properties. Toward this, end-functional −OH/−NH groups in P-UT and P-UT−UR were reacted with pentafluorophenyl isocyanate (PFI) to form PFI−P-UT and PFI−P-UT−UR (PFI-functionalized polyurea could not be synthesized because P-UR was not soluble in DMF solvent in order to carry out the reaction). From the FTIR spectra of PFI−P-UT (Figure S8), all the peaks and peak values remain unchanged when compared to those of the P-

Figure 9. Schematic representation of the formation of filaments in P-UT−UR after functionalization.

UT spectrum. The extent of H-bonding is also comparable. However, when the spectra of PFI−P-UT−UR and P-UT−UR are compared (Figure S9), a drastic difference is found. The heavily H-bonded broad peak at 3316 and 3211 cm^{-1} in P-UT−UR is narrowed and shifted to 3342 and 3219 cm^{-1} after functionalization. This indicates the reduction of H-bonding in PFI−P-UT−UR. Thus, it can be finally confirmed that −N−H···O−H H-bonding in P-UT−UR is stronger compared to homoatomic H-bonding. Hence, functionalization of P-UT to PFI−P-UT does not indicate any key changes in FTIR, but functionalization of P-UT−UR to PFI−P-UT−UR shows a notable change due to the hindrance of highly stable and strong heteroatomic H-bonding (Figure S10).

The surface morphology of PFI−P-UT and PFI−P-UT−UR was studied using FESEM analysis (Figure 8a). After functionalization, the spherulitic structure of P-UT−UR was changed to a fibrillar-/filament-like structure. PFI−P-UT−UR displayed filaments of length ∼2−3 μm in contrast to the interconnected nanospherulitic structure observed for P-UT−UR. The heavily H-bonded P-UT−UR having heteroatomic bonding leads to microphase separation and results in a porous web-like structure. However, this highly stable H-bonding is disturbed during the functionalization and the bonding sites/strength is altered, which lead to a different bonding in the new functionalized polymer having a more rigid filament-like structure, due to decrease/variation in H-bonding sites/strength. Attempts were made to characterize the morphology

Scheme 1. Synthesis of P-UT, P-UR, and P-UT−UR Polymers Performed at 125 °C at Inert Temperature
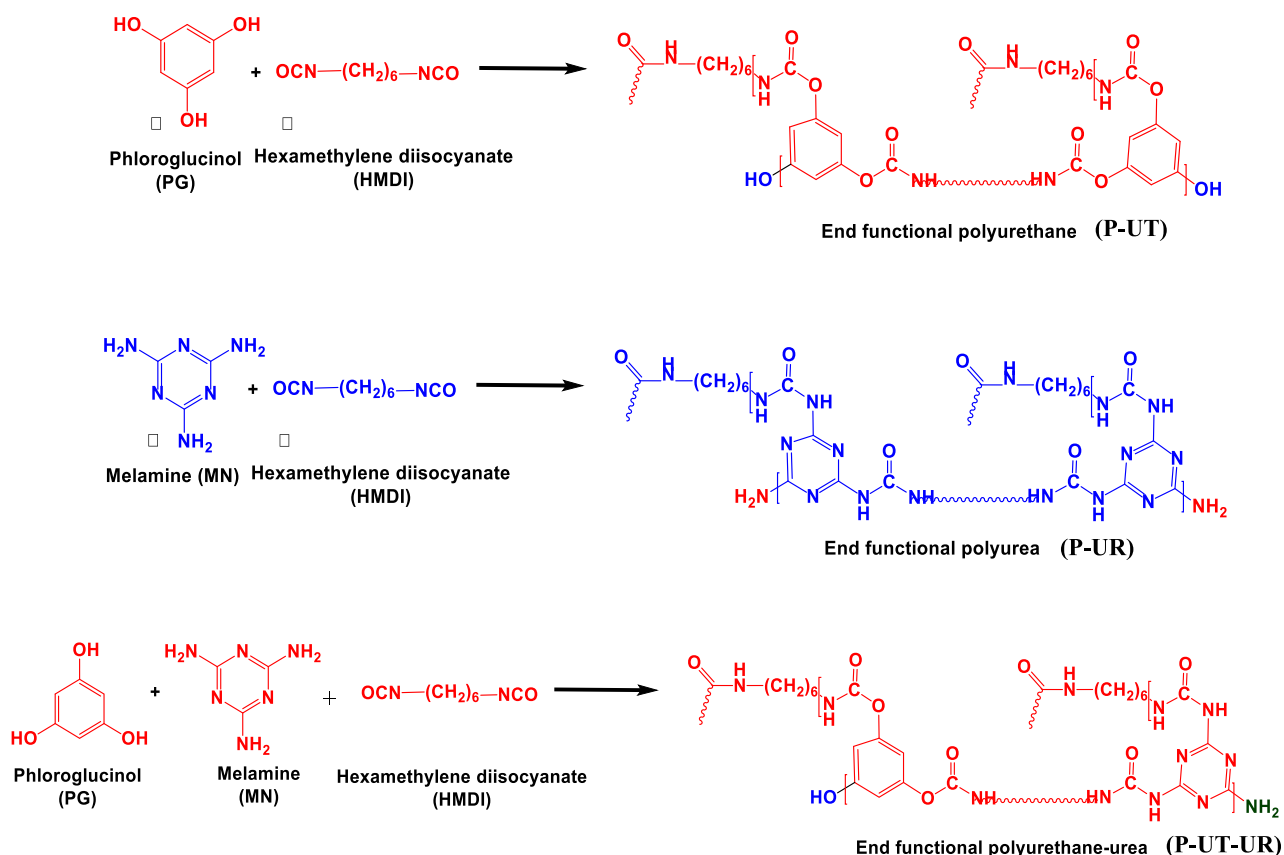

using AFM, but due to the nature of the surface features, the cantilever could not be properly engaged with the sample in the contact mode and could not extract much information about the surface parameters. However, the phase image (Figure 8b,c) obtained by tapping mode analysis of the films revealed that there was no phase separation. The change in the morphology from porous to fibrillar/filament after functionalization (Figure 9) can be enlightened by the possibility of self-assembly and end folding rearrangement during the process. Due to the presence of a highly electronegative fluorine group in pentafluorophenyl isocyanate, there is a possibility of excessive heteroatomic hydrogen bonding in the polymer after functionalization. This results in self-aggregation and end folding, resulting in the formation of a rigid filament structure.

Surface aggregation studies were done using static CA (Figure S11). From the CA readings, P-UT shows an initial CA of 113°, which is reduced to 80° in PFI−P-UT (hydrophobic to hydrophilic). This can be explained on the basis of the morphology changes after functionalization. It can also be inferred that PFI−P-UT has more H-bonding than P-UT. The reverse is observed in the case of PFI−P-UT−UR. Here, P-UT−UR showed an initial CA of 81°, which increases to ∼90° after functionalization. The increased CA of PFI−P-UT−UR may be due to the presence of microfilament projections in its morphology. The UV−visible spectra of the PFI−P-UT and PFI−P-UT−UR films were recorded and compared with those of P-UT and P-UT−UR, respectively (Figure S12a,b). In both the cases, the transparency of the film gets decreased after functionalization. In the first case, for PFI−P-UT, the initial transparency decreased from 56 to 36% after functionalization. However, reverse is observed in the

case of PFI−P-UT−UR. Here, the transparency increased from 44 to 50% after functionalization. This study can further be used for supporting the previously said theory that P-UT−UR is heavily H-bonded and the H-bonding is lost after functionalization. The Figure S12 inset shows the photographs of P-UT, PFI−P-UT, P-UT−UR, and PFI−P-UT−UR films.

3. CONCLUSIONS

End-functional P-UT, P-UR, and P-UT−UR hybrid were synthesized from phloroglucinol/melamine and hexamethylene diisocyanate. P-UT and the P-UT−UR hybrid formed films, whereas P-UR did not. FT-IR revealed the presence of extensive H-bonding in the P-UT−UR hybrid vis- à-vis P-UT and P-UR. The hybrid featured nanoporous spherulitic structures, whereas other two polymers did not display any peculiar morphology. However, on interaction with solvents of varying hydrophobic strengths such as water/THF, the morphology changed. The rationale for the exceptionally different morphology and assembly observed in hybrids may be due to the heteroatomic H-bonding involving −N−H···O−H. Heteroatomic H-bonding forms a strong secondary interaction compared to homoatomic H-bonding involving −O−H···O−H and −N−H···N−H bonding. In another approach, end-functional polymers were end capped by a reaction with monoisocyanate, which gave an easy route to achieve a nanofilament-rich polymer. The hybrid responded further tightening of the polymer via "end-group capping", which leads to the closing of pores and further extension of assembly that resulted in a nanofilament microstructure. This work exemplifies that subtle changes in the polymeric structure

Scheme 2. Synthesis of End-Terminated PFI–P-UT and PFI–P-UT–UR from Previously Synthesized P-UT and P-UT–UR End-Functional Polymers
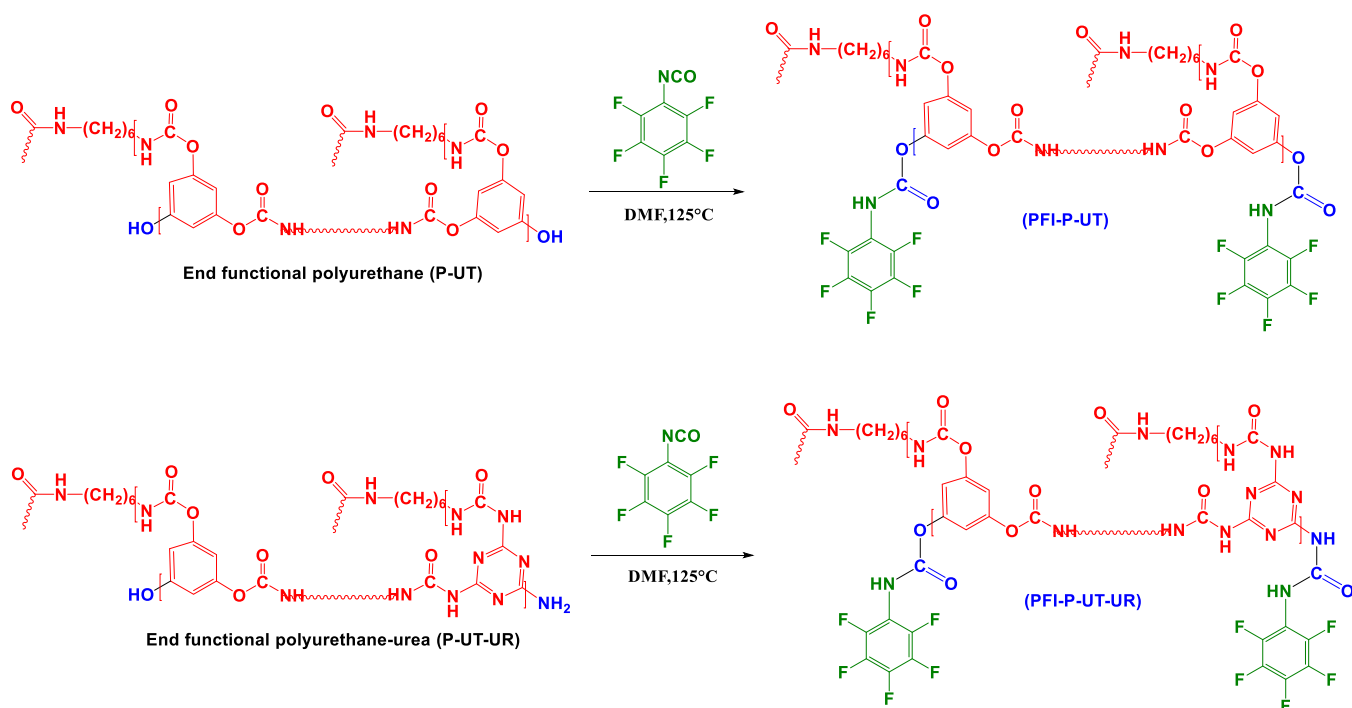
can offer exciting nano-ordered morphologies, which are attributed to heteroatom H-bonding.

4. EXPERIMENTAL SECTION

4.1. Materials. Phloroglucinol (98%, Avra Pvt. Ltd, India), melamine (98%, Avra Pvt. Ltd, India), hexamethylene diisocyanate (98%, Sigma-Aldrich, Germany), pentafluoro isocyanate (97%, Sigma-Aldrich, Germany), dimethyl formamide (≥99%, Central Drug House (P) Ltd.), acetone (≥99.5%, Sigma-Aldrich), methyl ethyl ketone (≥99%, Sigma-Aldrich), and tetrahydrofuran (≥99.9%, Sigma-Aldrich) were used as received. All the reagents were used as such without further purification.

4.2. Methods. *4.2.1. Synthesis of Functional Polyurethane (P-UT).* End functional polyurethane (P-UT) was synthesized as follows. Hexamethylene diisocyanate (1.5 mol) in 25 mL of DMF solvent was taken in a 500 mL round bottom flask. Phloroglucinol (1.3 mol) was dissolved in DMF (25 mL), which resulted in a clear solution. Dropwise addition of phloroglucinol solution from the dropping funnel to the isocyanate solution was conducted at 125 °C with continuous stirring under a N$_2$ atmosphere. The reaction was continued for 5 h with continuous stirring. After ensuring the complete absence of the −NCO group (from FTIR, the absence of the peak at 2270 cm^{-1} corresponds to the −NCO group), the hot clear solution was poured dropwise with continuous stirring to about 3 L of ice cold water, where the polymer was precipitated. The precipitate was filtered and dried at 120 °C under vacuum for 18 h. The final dried product was subjected to various analyses such as FTIR, DSC, thermogravimetric analysis (TGA), X-ray diffraction, FESEM, and so forth. Similarly, functional polyurea (P-UR) was synthesized using melamine and hexamethylene diisocyanate as reactants under the same reaction conditions as those used for P-UT. End functional polyurethane−urea (P-UT−UR) was synthesized by

employing phloroglucinol and melamine in the molar counts (0.97: 0.33). The synthesis schemes of all the above polymers are shown in Scheme 1.

4.2.2. Synthesis of Pentafluorophenyl Isocyanate-Terminated Polyurethane (PFI−P-UT). The obtained P-UT (1 mol) was dissolved in a minimum amount of DMF solution to form a clear solution (apparatus: 250 mL round bottom flask). 1.0 mol pentafluoro isocyanate was taken in a dropping funnel and added dropwise to an RB flask at 125 °C with continuous stirring under a N$_2$ atmosphere. After 5 h, the clear reaction mixture was poured to 3 L of ice cold water with vigorous stirring to form a precipitate. The precipitate was filtered and dried at 120 °C under vacuum for 18 h and subjected to various analyses. Similarly, the pentafluorophenyl isocyanate-terminated polyurethane−urea hybrid (PFI−P-UT−UR) was synthesized from P-UT−UR (1 mol) by following the same procedure as discussed above. The final precipitate was filtered and dried at 120 °C under vacuum. Scheme 2 shows the synthesis of PFI−P-UT and PFI−P-UT−UR.

4.3. Instrumental Techniques. FT-IR characterization of polymers was performed using a PerkinElmer Spectrum GX-A FTIR spectrophotometer. The analysis was carried out in the wavenumber range of 4000−400 cm^{-1} with a resolution of 4 cm^{-1}. ^{1}H NMR spectroscopy of polymers was carried out using a Bruker AVANCE spectrometer with CDCl$_3$ as solvent at a frequency of 300 MHz. TGA was carried out on a TA instrument, model SDT-2960. The temperature range of the analysis was 30−900 °C in a nitrogen atmosphere at a heating rate of 10 °C per minute. DSC studies were conducted on a TA instrument model 2920 modulated differential scanning calorimeter at a heating rate of 10 °C/min under a N$_2$ atmosphere. The surface morphology of materials was traced by FESEM on a Hitachi SU6600 variable pressure field-emission scanning electron microscope instrument. AFM analysis was carried out on an AFM instrument (Agilent

Technologies 5500). The static CAs of the P-UT films were measured with a Data Physics contact angle instrument OCA85 15EC (Drop size-5 μL, curve-fitting method). The transparency of P-UTs was measured by solid-state UV−vis spectroscopy using a PerkinElmer LAMDA 950 instrument.

■ ASSOCIATED CONTENT

Ⓢ Supporting Information

The Supporting Information is available free of charge at https://pubs.acs.org/doi/10.1021/acsomega.1c06888.

Glass-transition temperature (T_g) and softening point of P-UT, P-UR, and P-UT−UR; FTIR spectra of the BC-PUU hybrid and P-UT−UR; FESEM image of the BC-PUU hybrid; FTIR spectra of P-UT in various solvents; FTIR spectra of P-UR in various solvents; FTIR spectra of P-UT−UR in various solvents; Hansen solubility parameter of solvents used in this study; comparison of the FTIR spectra of PFI−P-UT and P-UT; comparison of the FTIR spectra of PFI−P-UT−UR and P-UT−UR; proposed mechanism of H-bonding in the BC-PUU hybrid; CAs of PFI−P-UT and PFI−P-UT−UR with respect to the time of contact; and transparency of PFI−P-UT and PFI−P-UT−UR films studied using UV−vis spectra (PDF)

■ AUTHOR INFORMATION

Corresponding Author

Santhosh Kumar Kalamblayil Sankaranarayanan − *Polymers and Special Chemicals Division, Vikram Sarabhai Space Centre, Thiruvananthapuram 695022, India;* ⓘ orcid.org/0000-0002-7891-7113; Email: santhoshkshankar@yahoo.com

Authors

Rashmi Edachery Veetil − *Polymers and Special Chemicals Division, Vikram Sarabhai Space Centre, Thiruvananthapuram 695022, India*

Bhuvaneswari Soundiraraju − *Analytical and Spectroscopy Division, Vikram Sarabhai Space Centre, Thiruvananthapuram 695022, India;* ⓘ orcid.org/0000-0001-8531-8904

Dona Mathew − *Polymers and Special Chemicals Division, Vikram Sarabhai Space Centre, Thiruvananthapuram 695022, India*

Complete contact information is available at:
https://pubs.acs.org/10.1021/acsomega.1c06888

Notes

The authors declare no competing financial interest.

■ ACKNOWLEDGMENTS

■ REFERENCES

(1) Hassanajili, S.; Khademi, M.; Keshavarz, P. Influence of various types of silica nanoparticles on permeation properties of polyurethane/silica mixed matrix membranes. *J. Membr. Sci.* **2014**, *453*, 369−383.

(2) Jia, S.; Qu, J.; Wu, C.; Liu, W.; Chen, R.; Zhai, S.; Huang, Z.; Chen, F. Novel dynamic elongational flow procedure for reinforcing strong, tough, thermally stable polypropylene/thermoplastic polyurethane blends. *Langmuir* **2013**, *29*, 13509−13517.

(3) Fu, H.-L.; Hong, Y.; Little, S. R.; Wagner, W. R. Collagenase-labile polyurethane urea synthesis and processing into hollow fiber membranes. *Biomacromolecules* **2014**, *15*, 2924−2932.

(4) Wang, S.-K.; Sung, C. S. P. Fluorescence and IR Characterization of Cure in Polyurea, Polyurethane, and Polyurethane− Urea. *Macromolecules* **2002**, *35*, 883−888.

(5) Breucker, L.; Landfester, K.; Taden, A. Phosphonic acid-functionalized polyurethane dispersions with improved adhesion properties. *ACS Appl. Mater. Interfaces* **2015**, *7*, 24641−24648.

(6) Mattia, J.; Painter, P. A Comparison of Hydrogen Bonding and Order in a Polyurethane and Poly (urethane− urea) and Their Blends with Poly (ethylene glycol). *Macromolecules* **2007**, *40*, 1546−1554.

(7) Rao, J.; Păunescu, E.; Mirmohades, M.; Gadwal, I.; Khaydarov, A.; Hawker, C. J.; Bang, J.; Khan, A. Supramolecular mimics of phase separating covalent diblock copolymers. *Polym. Chem.* **2012**, *3*, 2050−2056.

(8) Oprea, S. Novel quinoline-based polyurethane elastomers. The effect of the hard segment structure in properties enhancement. *J. Polym. Res.* **2012**, *19*, 9767.

(9) Ma, Z.; Hong, Y.; Nelson, D. M.; Pichamuthu, J. E.; Leeson, C. E.; Wagner, W. R. Biodegradable polyurethane ureas with variable polyester or polycarbonate soft segments: Effects of crystallinity, molecular weight, and composition on mechanical properties. *Biomacromolecules* **2011**, *12*, 3265−3274.

(10) Yilgör, I.; Yilgör, E.; Wilkes, G. L. Critical parameters in designing segmented polyurethanes and their effect on morphology and properties: A comprehensive review. *Polymer* **2015**, *58*, A1−A36.

(11) Wen, J.; Somorjai, G.; Lim, F.; Ward, R. XPS study of surface composition of a segmented polyurethane block copolymer modified by PDMS end groups and its blends with phenoxy. *Macromolecules* **1997**, *30*, 7206−7213.

(12) Członka, S.; Strąkowska, A.; Strzelec, K.; Kairytė, A.; Vaitkus, S. Composites of rigid polyurethane foams and silica powder filler enhanced with ionic liquid. *Polym. Test.* **2019**, *75*, 12−25.

(13) Edachery Veetil, R.; Vijayalakshmi, K. P.; Srinivas, C.; Mathew, D.; Kalamblayil Sankaranarayanan, S. K. Soft segment-free functional polyurethane: A versatile candidate for heat-healability, non-dissociative mechanism, and high elongation adhesive materials. *Polym. Adv. Technol.* **2021**, *32*, 3523−3534.

(14) Koberstein, J. T.; Gancarz, I.; Clarke, T. C. The effects of morphological transitions on hydrogen bonding in polyurethanes: Preliminary results of simultaneous DSC−FTIR experiments. *J. Polym. Sci., Part B: Polym. Phys.* **1986**, *24*, 2487−2498.

(15) Bai, S.; Wang, Z.; Zhang, X.; Wang, B. Hydrogen-bonding-directed layer-by-layer films: effect of electrostatic interaction on the microporous morphology variation. *Langmuir* **2004**, *20*, 11828−11832.

(16) Lu, G.; Zhang, X.; Cai, X.; Jiang, J. Tuning the morphology of self-assembled nanostructures of amphiphilic tetra (p-hydroxyphenyl) porphyrins with hydrogen bonding and metal−ligand coordination bonding. *J. Mater. Chem. A* **2009**, *19*, 2417−2424.

(17) Goddard, R. J.; Cooper, S. L. Polyurethane cationomers with pendant trialkylammonium groups: Effects of ion content, alkyl group, and neutralizing anion. *J. Polym. Sci., Part B: Polym. Phys.* **1994**, *32*, 1557−1571.

(18) Chiche, D.; Chizallet, C.; Durupthy, O.; Chanéac, C.; Revel, R.; Raybaud, P.; Jolivet, J.-P. Growth of boehmite particles in the presence of xylitol: morphology oriented by the nest effect of hydrogen bonding. *Phys. Chem. Chem. Phys.* **2009**, *11*, 11310−11323.

(19) Liu, Y.; Zhao, J.; Peng, Y.; Luo, J.; Cao, L.; Liu, X. Comparative Study on the Properties of Epoxy Derived from Aromatic and Heteroaromatic Compounds: The Role of Hydrogen Bonding. *Ind. Eng. Chem. Res.* **2020**, *59*, 1914−1924.

(20) Hutchins, K. M. Functional materials based on molecules with hydrogen-bonding ability: applications to drug co-crystals and polymer complexes. *R. Soc. Open Sci.* 2018, 5, 180564.

(21) Liu, C.; Wang, J.; Li, J.; Zeng, M.; Luo, R.; Shen, J.; Sun, X.; Han, W.; Wang, L. Synthesis of N-doped hollow-structured mesoporous carbon nanospheres for high-performance supercapacitors. *ACS Appl. Mater. Interfaces* 2016, 8, 7194−7204.

(22) Madhavan, P.; Peinemann, K.-V.; Nunes, S. P. Complexation-tailored morphology of asymmetric block copolymer membranes. *ACS Appl. Mater. Interfaces* 2013, 5, 7152−7159.

(23) Singh, K. P.; Mishra, A.; Kumar, N.; Tripathi, D. N.; Shami, T. C. Evaluation of thermal, morphological and flame-retardant properties of thermoplastic polyurethane/polyphosphazene blends. *Polym. Bull.* 2018, 75, 2415−2430.

(24) Zhu, Y.; Liu, L.; Du, J. Probing into homopolymer self-assembly: how does hydrogen bonding influence morphology? *Macromolecules* 2013, 46, 194−203.

(25) David, J. G.; Hallam, H. E. Hydrogen-bonding studies of thiophenols. *Spectrochim. Acta* 1965, 21, 841−850.

(26) Johansson, A.; Kollman, P.; Rothenberg, S.; McKelvey, J. Hydrogen bonding ability of the amide group. *J. Am. Chem. Soc.* 1974, 96, 3794−3800.

(27) Ocheje, M. U.; Charron, B. P.; Cheng, Y.-H.; Chuang, C.-H.; Soldera, A.; Chiu, Y.-C.; Rondeau-Gagné, S. Amide-containing alkyl chains in conjugated polymers: effect on self-assembly and electronic properties. *Macromolecules* 2018, 51, 1336−1344.

(28) Liu, J.; McCullough, R. D. End group modification of regioregular polythiophene through postpolymerization functionalization. *Macromolecules* 2002, 35, 9882−9889.

(29) Hsieh, T.-T.; Hsieh, K.-H.; Simon, G. P.; Tiu, C. Inter-penetrating polymer networks of 2-hydroxyethyl methacrylate terminated polyurethanes and polyurethanes. *Polymer* 1999, 40, 3153−3163.

(30) Boufflet, P.; Casey, A.; Xia, Y.; Stavrinou, P. N.; Heeney, M. Pentafluorobenzene end-group as a versatile handle for para fluoro "click" functionalization of polythiophenes. *Chem. Sci.* 2017, 8, 2215−2225.

(31) Kuzmyn, A. R.; De Los Santos Pereira, A.; Pop-Georgievski, O.; Bruns, M.; Brynda, E.; Rodriguez-Emmenegger, C. Exploiting end group functionalization for the design of antifouling bioactive brushes. *Polym. Chem.* 2014, 5, 4124−4131.

(32) Li, X.; Li, J.; Wei, W.; Yang, F.; Wu, M.; Wu, Q.; Xie, T.; Chen, Y. Enhanced Mechanochemiluminescence from End-Functionalized Polyurethanes with Multiple Hydrogen Bonds. *Macromolecules* 2021, 54, 1557−1563.

(33) Fridman, I. D.; Thomas, E. L. Morphology of crystalline polyurethane hard segment domains and spherulites. *Polymer* 1980, 21, 388−392.

(34) Shi, R.; Wang, B.; Yan, Z.; Wang, Z.; Dong, L. Effect of surface topography parameters on friction and wear of random rough surface. *Materials* 2019, 12, 2762.

(35) Meireles, A. B.; Bastos, F. d. S.; Cornacchia, T. P.; Ferreira, J. A.; Las Casas, E. B. d. Enamel wear characterization based on a skewness and kurtosis surface roughness evaluation. *Biotribology* 2015, 1−2, 35−41.

(36) Macek, W.; Rozumek, D.; Królczyk, G. M. Surface topography analysis based on fatigue fractures obtained with bending of the 2017A-T4 alloy. *Measurement* 2020, 152, 107347.

(37) Hamelin, A.; Weaver, M. J. Dependence of the kinetics of proton reduction at gold electrodes on the surface cyrstallographic orientation. *J. Electroanal. Chem. Interfacial Electrochem.* 1987, 223, 171−184.

(38) Houton, K. A. *Use of Heterocomplementary Hydrogen Bonding Motifs for Supramolecular Materials Chemistry*; University of Leeds, 2015.

(39) Yang, A.; Huntington, M. D.; Cardinal, M. F.; Masango, S. S.; Van Duyne, R. P.; Odom, T. W. Hetero-oligomer nanoparticle arrays for plasmon-enhanced hydrogen sensing. *ACS Nano* 2014, 8, 7639−7647.

(40) Chang, J.; Zuo, J.; Zhang, L.; O'Brien, G. S.; Chung, T.-S. Using green solvent, triethyl phosphate (TEP), to fabricate highly porous PVDF hollow fiber membranes for membrane distillation. *J. Membr. Sci.* 2017, 539, 295−304.

(41) Gopalan, S.-A.; Seo, M.-H.; Anantha-Iyengar, G.; Han, B.; Lee, S.-W.; Kwon, D.-H.; Lee, S.-H.; Kang, S.-W. Mild wetting poor solvent induced hydrogen bonding interactions for improved performance in bulk heterojunction solar cells. *J. Mater. Chem. A* 2014, 2, 2174−2186.

(42) Weissbuch, I.; Torbeev, V. Y.; Leiserowitz, L.; Lahav, M. Solvent effect on crystal polymorphism: why addition of methanol or ethanol to aqueous solutions induces the precipitation of the least stable β form of glycine. *Angew. Chem.* 2005, 117, 3290−3293.

(43) Zuaznabar-Gardona, J. C.; Fragoso, A. Determination of the Hansen solubility parameters of carbon nano-onions and prediction of their dispersibility in organic solvents. *J. Mol. Liq.* 2019, 294, 111646.

(44) del Pilar Sánchez-Camargo, A.; Bueno, M.; Parada-Alfonso, F.; Cifuentes, A.; Ibáñez, E. Hansen solubility parameters for selection of green extraction solvents. *TrAC, Trends Anal. Chem.* 2019, 118, 227−237.

(45) Novo, L. P.; Curvelo, A. A. S. Hansen solubility parameters: a tool for solvent selection for organosolv delignification. *Ind. Eng. Chem. Res.* 2019, 58, 14520−14527.

(46) Liu, Z.; Wu, B.; Xiang, D.; Zhu, Y. Effect of solvents on morphology and photocatalytic activity of BiOBr synthesized by solvothermal method. *Mater. Res. Bull.* 2012, 47, 3753−3757.

(47) Joshi, D. P.; Pant, G.; Arora, N.; Nainwal, S. Effect of solvents on morphology, magnetic and dielectric properties of (α-Fe2O3@ SiO2) core-shell nanoparticles. *Heliyon* 2017, 3, No. e00253.

(48) Bhat, M. N.; Dharmaprakash, S. Effect of solvents on the growth morphology and physical characteristics of nonlinear optical γ-glycine crystals. *J. Cryst. Growth* 2002, 242, 245−252.

(49) Lofgreen, J. E.; Ozin, G. A. Controlling morphology and porosity to improve performance of molecularly imprinted sol−gel silica. *Chem. Soc. Rev.* 2014, 43, 911−933.

(50) Weber, J.; Du, N.; Guiver, M. D. Influence of intermolecular interactions on the observable porosity in intrinsically microporous polymers. *Macromolecules* 2011, 44, 1763−1767.

(51) Wang, A.; Cui, L.; Debnath, S.; Dong, Q.; Yan, X.; Zhang, X.; Ulijn, R. V.; Bai, S. Tuning supramolecular structure and functions of peptide bola-amphiphile by solvent evaporation−dissolution. *ACS Appl. Mater. Interfaces* 2017, 9, 21390−21396.